Absolute isotropic spectral intensities in collision-induced light scattering by helium pairs over a large frequency domain

Florent Rachet, Yves Le Duff, Christophe Guillot-Noël, and Michael Chrysos
Laboratoire des Propriétés Optiques des Matériaux et Applications, Université d'Angers, EP CNRS 130, 2, Boulevard Lavoisier, 49045 Angers, Cedex, France
(Received 1 February 2000; published 3 May 2000)

We measured the polarized binary collision-induced light scattering spectrum from room-temperature gaseous helium over the greatly extended spectral domain $\nu = 5-1200\,\mathrm{cm}^{-1}$, and then deduced the isotropic spectrum that we report in the interval $\nu = 100-1200\,\mathrm{cm}^{-1}$. Our experimental results were calibrated on an absolute scale. These data were compared to those from quantum-mechanical computations, where use of advanced induced-polarizability incremental traces was made. This comparison enabled us to check several trace models and to show that for certain *ab initio* ones the computed spectra agree well with our measurements. As was borne out from our computations the main contributions to the spectral intensities come from the *exchange* component of the incremental trace and its negative mixing with the rest of the trace components.

PACS number(s): 33.20.Fb, 34.30.+h

I. INTRODUCTION

When a light beam strikes an isolated atom, the system responds by a single peak—the so-called Rayleigh peak—at the same frequency as that of the incident light. When a sample of interacting atoms is instead handled, interaction-induced polarizabilities between colliding atoms give rise to a collision-induced light scattering (CILS) spectrum. This spectrum surrounds the Rayleigh peak and is extended over both the Stokes and the anti-Stokes spectral sides. CILS spectra constitute the fingerprints of collective polarizabilities [1–3]. More specifically, because of interactions between constituents of the sample, the latter can be seen as a cluster with a polarizability differing from the sum of the individual atomic polarizabilities. However, for a sufficiently low density of the medium only binary interactions are relevant.

Among the different atomic systems helium is an intriguing candidate for theory since, due to its simple electronic structure, it allows for a refined and a realistic description as well as for the detailed understanding of purely quantum mechanisms. It turns out that when frequency-integrated intensities are concerned, the CILS from helium pairs is mainly generated by the *anisotropy* β, of the interaction-induced polarizability tensor, whose fingerprint is the *depolarized* spectrum. However, frequency-resolved CILS studies have shown that an *isotropic* component generated by the *incremental trace* $\Delta\alpha$, of the interaction-induced polarizability tensor manifests itself too [1].

The helium isotropic CILS spectrum is extremely weak. To give an idea, at frequencies close to the Rayleigh peak its intensity compared to that of the corresponding argon spectrum is weaker by two orders of magnitude [4,5]. There is no doubt that the essential obstacle in the study of the CILS far spectral wings is the difficulty to measure reliably such weak signals. In addition, due to the weak intensities of the signal, residual impurities mixing with helium may substantially distort the line shape, even at very low concentrations. Despite these difficulties, as accurate as possible knowledge of the isotropic far spectral wing is particularly valuable. It is because this serves as a sensitive probe of the pair polarizability when the helium atoms are in very close approach and therefore provides information on the electro-optical properties of the medium (refractive index, dielectric constant) via the second virial dielectric coefficient.

The helium isotropic spectrum was first reported in the interval $20-320\ \mathrm{cm}^{-1}$ by Proffitt *et al.* [6–9]. Their measurements, performed for a single density of the sample (30.5 amagat), remain thus far the only experimental results available in the literature. Here we report new measurements over a large spectral range corresponding to an extension of the thus far explored domain by almost four times. This extension becomes possible by using an experimental setup especially adapted to the detection of an extremely low photon flux. The comparison of our experimental data with theoretical spectra (obtained by using a fully quantum computation based on a modern approach) allows for the more complete comprehension of the interaction mechanism through improved pair polarizability models, and contributes to the knowledge of certain macroscopic electro-optical properties of the gas.

The paper is organized as follows. Experimental conditions are briefly described in Sec. II; Sec. III deals with the theoretical models available in the literature for the simulation of the isotropic spectrum, as well as with our computational implementation. The experimental implementation and measurements are given in Sec. IV, while a discussion concerning the isotropic intensities is made in Sec. V. Finally, concluding remarks are given in Sec. VI.

II. EXPERIMENTAL SETUP

For the registration of the CILS spectrum, a typical Raman experiment is set up operating with a right angle scattering geometry. The 514.5-nm green spectral line of an argon ion laser is used, whose power is stabilized at 2 W for all experiments. The polarization of the laser beam is perpendicular to the scattering plane, that is the plane formed by the incident beam and the direction in which the scattered light is detected. When a change of the incident beam's polariza-

tion is desired so that the latter is parallel to the scattering plane, a half-wave plate and a glan polarizer are employed. The gaseous helium sample is contained in a four-window high-pressure cell at room temperature. Depending on the gas pressure, fused silica or sapphire windows are used. In order to reduce the parasitic light due to reflections inside the cell we make use of a blackened tube with nonperiodic screw thread and diaphragms inside the cell, as well as of multilayer antireflection coatings for its windows. The registration of the polarized $Q_1(1)$ rotovibrational line of H_2 (at 4155 cm^{-1}) ensures that no polarization defect is produced by the windows. To reduce the contribution to the scattering intensities of signals arising from the impurities, we use highly purified helium gas (Air Liquide Co.) with total residual impurities less than 1 ppm. Densities are deduced from measurements of the product PV against pressure P, with T as a parameter [10,11].

Just before entering the double monochromator, the scattered beam crosses a quartz scrambler so that the different polarizations of the light signal are mixed up. An asymmetric Czerny-Turner optical configuration with additive dispersion, supplied with two 1800 grooves/mm holographic gratings, is used for the spectrometer.

The vertical I_V and the horizontal I_H spectral components are recorded with the polarization of the incident beam perpendicular and parallel to the scattering plane, respectively. For an aperture angle of the scattered beam close to zero, the isotropic spectrum is deduced from a linear combination of the two registred components [12]:

$$I_{\mathrm{iso}}(\nu)=I_V(\nu)-\tfrac{7}{6}I_H(\nu). \tag{1}$$

Two different detection devices are used. A photomultiplier (PM) for low and intermediate frequencies, and a multichannel charged coupled device (CCD) camera for the far spectral wing. As regards the PM, the following two frequency ranges are covered: 5–400 cm^{-1} for I_H and 5–640 cm^{-1} for I_V. The frequency ranges for the CCD are 320–680 cm^{-1} for I_H and 320–1200 cm^{-1} for I_V. This is the first time such a complementary detection has been implemented in CILS.

The transmission curves of the entire detection device are beforehand registered by means of a calibrated OSRAM spectral lamp, delivering white light at temperature (2071 ± 17) K. In this way, a spectral correction is made on each experimental intensity, so that the variation of the sensitivity of our apparatus with the wavelength is taken into account. The uncertainty related to the spectral calibration of the detection device amounts to $\pm 2\%$. The width of the slits of the double monochromator is chosen to be a function of the signal intensity and of the resolution constraints. More specifically, for the PM, a resolution of 2 cm^{-1} is taken for signals close to the Rayleigh peak and 10 cm^{-1} elsewhere. For the CCD, the resolution is fixed to 2.5 cm^{-1}.

III. THEORY AND NUMERICAL IMPLEMENTATION

A. The He_2 interaction-induced trace

The collision-induced polarizability is a function of the internuclear separation r. What is probed by the isotropic CILS spectrum is one of the polarizability tensor's invariants, called incremental trace $\Delta\alpha(r)$. In this work, the emphasis is put on three *ab initio* models of $\Delta\alpha$. The first, according to Dacre and Frommhold (denoted DF), has been known for a long time [13,14]. The remaining two models, proposed by Bishop and Dupuis [15] and by Moszynski, Heijmen, Wormer, and van der Avoird (denoted MHWA) [16], are more up to date. Let us briefly describe their main characteristics.

The DF model was obtained from a large-scale *ab initio* computation based on a mixed self-consistent field (SCF) plus configuration interaction (CI) approach. The contribution of the electronic correlation was taken into account through CI. In the interval 3–10 Bohr, the numerical trace was converted to a piecewise analytic function by interpolating the two corrected terms $\alpha_{\mathrm{SCF}}^{\mathrm{COR}}$ and $\alpha_{\mathrm{CI}}^{\mathrm{COR}}$, where the superscripted COR denotes ''counterpoise correction.'' Beyond 10 Bohr, the numerical incremental trace was extrapolated with the well established asymptotic law A_6/r^6, where $A_6=37.0a_0^9$ (a_0 stands for the Bohr radius).

There are three different models of incremental trace proposed by Bishop and Dupuis [15]. Here the MP2 model is chosen, denoted to this end by BD. In their *ab initio* calculation the electron-electron correlation effect was taken into account at the second-order Moller-Plessett MP2 theory. Beyond $r=13$ Bohr, the BD numerical incremental trace model joined the asymptotic limit A_6/r^6, with $A_6=39.29a_0^9$.

The MHWA *ab initio* model of Moszynski and coworkers was obtained by means of symmetry-adapted perturbation theory (SAPT). The induced incremental trace $\Delta\alpha_{\mathrm{MHWA}}$ was built from four partial contributions: the *polarization* $\Delta\alpha_{\mathrm{pol}}$, the *exchange* $\Delta\alpha_{\mathrm{exc}}$, the *induction* $\Delta\alpha_{\mathrm{ind}}$, and the *dispersion* $\Delta\alpha_{\mathrm{dis}}$. Both intra-atomic and interatomic correlation effects were taken into account in their computations. The *exchange* and *polarization* terms were described by a decaying exponential. The *induction* and *dispersion* contributions were represented by one or several multipolar terms multiplied by a damping Tang-Toennies-type function. Finally, overlap effects at short distances were described by a decreasing exponential function.

Here, we also check three other trace models, for the sake of completeness. (i) The incremental trace model of Certain and Fortune (denoted CF) [17], where a variational approach based on quantum theory was used to calculate a coefficient accounting for the long-distance London dispersion effects. (ii) The incremental trace model of Fortune and Certain (denoted FC) [18], where a coupled self-consistent field (SCF) calculation based on a finite field method was established. In their calculation, the contributions due to electronic correlation and dispersion effects were neglected whereas the attenuation of the *overlap* and *exchange* effects with increasing r was represented by a decaying exponential. (iii) The semiempirical incremental trace model proposed by Proffitt, Keto, and Frommhold (denoted PKF), conceived to fit the experimental isotropic spectrum of Frommhold's group [6–9]. In the two-terms expression, which compose this model, the first accounted for the dipole-induced-dipole (DID) contribution as well as for London dispersion effect

while an exponential second term described the *exchange* and *overlap* effects at short interatomic distances.

B. Spectral intensities: Computations

In order to compute spectra by helium pairs, we adopt a recently developed fully quantum numerical procedure. The wave functions are built step by step, according to the Fox-Goodwin propagative method, through outward propagation of the wave-function ratio at every pair of adjacent points defined on a spatial grid [19,20].

The absolute isotropic spectra are computed at temperature T by using the following formula [5,21,22]:

$$I_{\mathrm{iso}}(\nu)=hcL^3k_S^4\sum_{J=0,J\ \mathrm{even}}^{J_{\max}}(2J+1)\times\int_0^{E_{\max}}|\langle\psi_{E',J}|\Delta\alpha|\psi_{E,J}\rangle|^2\exp\left(-\frac{E}{k_BT}\right)dE. \tag{2}$$

The symbol k_S stands for the Stokes wave number of the scattered light, h is Planck's constant and c is the speed of the light. Constant L accounts for the thermal de Broglie wavelength, $L=h/\sqrt{2\pi\mu k_BT}$, with μ the reduced mass of He_2 and k_B Boltzmann's constant. The energy of the initial state is denoted by E and that of the final state by $E'=E+h\nu$, in the Stokes spectral side. Symbol $\psi_{E,J}$ designates the scattering wave function and $E_{\max}$ the maximum value of the energy that is required to obtain convergence of the integral.

The spatial grid goes from 3 Bohr to 150 Bohr. The upper bound in the integral over energy is fixed to 3000 cm^{-1} and the corresponding integration step ΔE to 15 cm^{-1}. The maximum angular momentum quantum number is taken $J_{\max}=100$. These numerical parameters provide convergence of total cross sections to within $<1\%$.

The Lennard-Jones 6–12 [23], HFD-B3-FCI1 [24], HFD-ID [25], SAPT1 [26,27], and r_{12}-MR-ACPF [28] interatomic potential models are checked: a brief comparison of these potentials is given below. For all computations, the advanced SAPT1 potential is used.

IV. EXPERIMENTAL IMPLEMENTATION AND MEASUREMENTS

Let us now focus on aspects concerning the acquisition and the treatment of the experimental data recorded at room temperature (294.5 ± 1) K by either the two detectors (PM and CCD).

For the low-frequency intensities, i.e., below $\nu=640\,\mathrm{cm}^{-1}$, we make use of a low dark-noise bialkali photomultiplier detector, cooled to $-5\,^{\circ}\mathrm{C}$ and followed by a discriminator and a photon counter. Densities up to 300 amagat are dealt with, that is a gas pressure going up to 386.5 bars [29]. To account for the weak intensities, long counting time intervals up to 40 min per registered frequency are used, so that the statistical uncertainty of the signal counts after subtraction of the dark counts is to within a few percent [30].

In order to deduce from our measurements *binary* He_2 intensities, the dependence of the scattering signal is studied at any frequency ν as a function of the sample's density ρ, and for both polarizations, horizontal and vertical. Since the scattering signal $I(\nu)$ can be viewed as the result of a power series expansion in ρ, we have

$$I(\nu)=I_0(\nu)+I_1(\nu)\rho+I_2(\nu)\rho^2+I_3(\nu)\rho^3+\cdots \tag{3}$$

with ν-dependent coefficients of particular physical interpretation. The first term $I_0(\nu)$ of the series is related to the dark noise of the photomultiplier, as well as to the signal of the empty cell once illuminated by the laser. The coefficient $I_1(\nu)$ refers to the signal coming from monomers since the corresponding term scales linearly with ρ. The term with $I_2(\nu)$ scales quadratically with ρ. It is interpreted as the contribution to the spectrum of colliding pairs, and the corresponding intensity provides the so-called binary spectrum of the gas. In what follows the subscript ''2'' will be suppressed from all quantities referred to spectral intensities for the sake of simplicity, implicitly meaning that $I_V(\nu)$, $I_H(\nu)$, and $I_{\mathrm{iso}}(\nu)$ refer to binary spectra. Higher-order terms, $I_3(\nu),I_4(\nu),\ldots$, represent ternary or higher-order spectra and arise from three-body collisions, four-body collisions, and so on. The study as a function of the density offers the advantage of enabling one to eliminate all parasitic light [in particular that due to the impurities, which scales linearly with ρ and thus contributes to $I_1(\nu)$] and extract the binary spectrum from the measurements.

The reported PM spectrum results from the analysis of 8–10 different spectra, each corresponding to a given gas density. As a criterion to determine the density working range we seek density regimes for which all terms beyond the quadratic one [in the series expansion of Eq. (3)] are negligibly small. On physical grounds, this property is the signature of purely binary interactions between atoms. More specifically, the upper bounds of the density intervals treated amount to 100 amagat, 140 amagat, 180 amagat, 220 amagat, and 300 amagat, for the spectral ranges 5–13 cm^{-1}, 15–37 cm^{-1}, 40–175 cm^{-1}, 200–300 cm^{-1}, and 325–640 cm^{-1}, respectively.

The calibration on an absolute scale of the spectral intensities in vertical polarization $I_V(\nu)$ is made by relating the binary He_2 relative experimental intensities $I_2(\nu)$ [see Eq. (3)], to the frequency integrated intensity $I_{\mathrm{int}}^{\mathrm{H_2}}$ of the H_2 Raman rotational line $S_0(0)$ that serves as Ref. [31]:

$$I_V(\nu)=\frac{14}{45}k_S^4\gamma^2P_J\frac{3(J+1)(J+2)}{2(2J+1)(2J+3)}\left(\frac{n'}{n^2}\right)\left(\frac{I_2(\nu)}{I_{\mathrm{int}}^{\mathrm{H_2}}}\right). \tag{4}$$

In this expression, n and n' are the number densities of helium and molecular hydrogen, respectively. P_J stands for the fractional population of the Jth rotational level of H_2 at the temperature of the experiment. Its computation is made by using molecular constants from Ref. [32]. The quantitiy γ $[=(3.18\pm0.03)\times10^{-25}\,\mathrm{cm}^3$ [33]] stands for the anisotropy of the rotational line $S_0(0)$ of H_2 taken at the laser wavelength. $I_2(\nu)$ is corrected by the transmission curve of the device. In view of the manner we defined the transmission factor, a k_S^4 law dependence of the scattered intensity is established. Finally, the quantity $I_{\mathrm{int}}^{\mathrm{H_2}}$ represents the frequency-

integrated intensity of the Raman line of H_2 that is chosen as an etalon at atmospheric pressure. In order to calibrate the spectral intensities in horizontal polarization, the symbol $I_V(\nu)$, on the left-hand side of Eq. (4), has to be replaced by $I_H(\nu)$, while the right-hand side has to be scaled by the factor 6/7.

According to the above-mentioned procedure, an external calibration is performed at 76 cm^{-1}, followed by a relative calibration for all the other frequencies ν. The calibrated intensity is defined as the average value of independent measurements, giving the values $I_H(\nu=76\,cm^{-1})=(1.34\pm0.11)\times10^{-57}\,cm^6$ and $I_V(\nu=76\,cm^{-1})=(1.69\pm0.14)\times10^{-57}cm^6$.

On the other hand, beyond $\nu=320\,cm^{-1}$, a Jobin Yvon Si chip CCD detector is used. The long side of its array, containing 1024×256 pixels, is oriented along the direction of the dispersion of the spectrograph. The chip is cooled to 140 K by liquid nitrogen, in order to maintain a very good dark current whose value is less than 0.1 photoelectron/pixel/h. The stored spectrum is composed of 1024 channels, each corresponding to a column of 256 vertically binned pixels. The chip is not totally illuminated by the scattered beam. The so-called blind parts, corresponding to 140 channels at each side of the grid, define the signal baseline, which is checked to be constant over the entire size of the grid. The acquisition procedure and the statistical treatment of the data, and in particular the way to eliminate the peaks due to the cosmic rays, are described in Ref. [34]. The statistical treatment is made on 7 or 11 measurements for every frequency, with a counting time comprised between 600 sec and 1500 sec per measurement. The illuminated pixels cover a block of about 160 cm^{-1}. Each block is calibrated independently on an absolute scale according to the method described above. In order to eliminate the parasitic light due to the Rayleigh peak, a holographic filter (supernotch filter of the Kaiser Optical Systems Society) [35,36] is introduced at the entrance of the spectrograph. To account for the rejection band of this filter, the frequency lower bound of the measurements is set at 320 cm^{-1}.

A preliminary analysis of the spectrum as a function of the density shows that in the frequency domain beyond 320 cm^{-1} the contribution of the impurities to the signal is negligible. In addition, as is shown in Fig. 1, it turns out that for densities $\leqslant$300 amagat only binary interactions are relevant in this frequency domain. Therefore, the working density of the sample is chosen at $\rho=280$ amagat ($\simeq$356 bars) for which the signal satisfies two requirements, i.e., it has a purely quadratic density dependence whereas its intensity is as high as possible. The binary spectra I_H and I_V obtained with the CCD are recorded at this single density of the sample.

The excellent sensitivity of this detector and the statistical procedure of the data acquisition enable one to extend the detection limit of a measurable signal and to attain sensitivities of about 1 photoelectron/pixel/week. We therefore manage to greatly extend the exploration of the far Stokes wing of the I_V spectrum to $\nu=1200\,cm^{-1}$. This performance should be compared with the previous limit of 320 cm^{-1} [6–9].

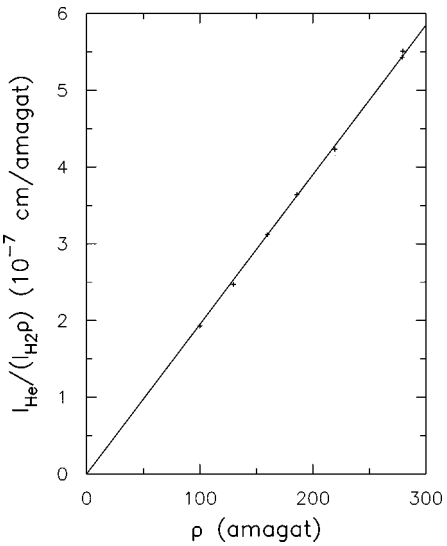

FIG. 1. Ratio of I_V divided by the density ρ and the integrated intensity of the $S_0(0)$ rotational Raman line of H_2 at 1 amagat, plotted as a function of ρ. These results, given for the frequency $\nu=320\,cm^{-1}$, have been obtained with the CCD detector. At $\rho=0$ the plotted function becomes zero, that is the indication of the absence of any parasitic signal due to impurities. Since the plotted ratio scales linearly with density, only binary interactions are relevant.

Figure 2 shows our experimental spectrum in vertical polarization $I_V(\nu)$. The measurements are illustrated on an absolute scale. The results obtained with the PM are represented by points. The lower bound of the reported spectrum is $\nu=5\,cm^{-1}$. This is the first time measurements this close to the Rayleigh peak have been taken for helium. The results

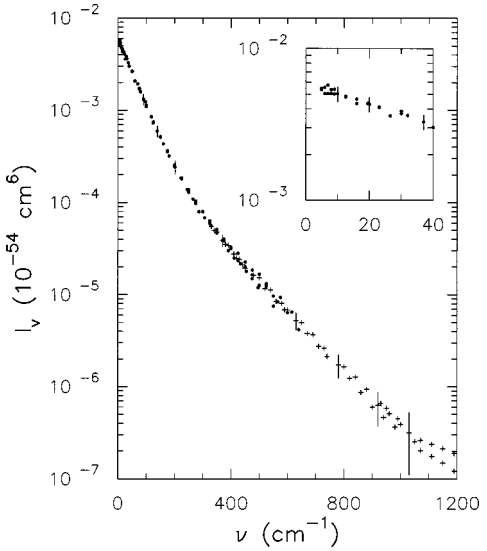

FIG. 2. Polarized CILS spectrum $I_V(\nu)$ on an absolute scale (cm^6), as a function of frequency ν. The points refer to measurements with PM and the crosses to those with CCD. As an indication, some representative error bars are given. In the inset, the low-frequency interval 5–40 cm^{-1} is given, showing the low dispersion of our measurements.

obtained with the CCD are represented by crosses. In the interval 320–640 cm^{-1}, where both detectors are operational, an excellent agreement is ascertained.

V. DISCUSSION

From the polarized intensities $I_V(\nu)$ measured in this work, and by using the depolarized intensities obtained recently by our group in the interval 5–680 cm^{-1} [37], we deduce the binary isotropic helium spectrum by taking into account the aperture half-angle of the scattered beam of our setup (8.1°). According to the general formula given in Ref. [9], we have

$$I_{\rm iso}(\nu) = -1.184 I_H(\nu) + 1.017 I_V(\nu). \tag{5}$$

Although the upper frequency bound for I_H amounts to 680 cm^{-1}, isotropic intensities up to $\nu = 1200\,cm^{-1}$ are deductable by making use of a surprising property the helium pair is found to reveal: As we have shown recently, the depolarization ratio of the CILS generated by helium pairs exhibits a continuously decreasing behavior with increasing ν, and beyond 600 cm^{-1} attains values very close to zero (0.03 at $\nu = 680\,cm^{-1}$) [38]. This exceptional finding has thus far never been observed in CILS spectra by other species [38]. The origin of this characteristic behavior has been attributed to an almost perfect cancellation between polarization and exchange pair polarizability contributions of the depolarized intensities in the very far wing [37]. This conclusion has been drawn from the quantum-mechanical computations we have done using the pair polarizability model of Moszynski *et al.* [16]. Given that the latter model well reproduces the experimental helium depolarization ratio throughout the entire domain probed [38], we assume that the depolarization ratio also remains close to zero for frequencies beyond 680 cm^{-1}. The contribution of I_H to the isotropic CILS intensities $I_{\rm iso}(\nu)$ can thus be neglected in Eq. (5) for frequencies beyond 680 cm^{-1}. This fact allows us to extend the knowledge of the isotropic spectrum to $\nu = 1200\,cm^{-1}$ that is the upper bound of the experimental polarized intensities. In Fig. 3, our experimental He_2 isotropic spectrum is plotted. The solid-line curve accounts for the best fit of our measurements between 100 cm^{-1} and 1200 cm^{-1}, as a guide to the eye. No measurements are given below 100 cm^{-1} because, there, the isotropic spectrum arises as the difference between two almost identical quantities, and therefore the resulting intensities are not reliable. In Table I, some values of the best fit are given on an absolute scale. Until the present work, the only experimental reference on the helium isotropic spectrum was that reported some time ago by Proffitt *et al.* on an absolute scale [6–9]. Figure 3 allows a comparison of our experimental spectrum with that of Proffitt *et al.* The substantial extension of the explored frequency domain is clearly seen and the great difference between the two spectra (in the common frequency interval) is stressed. However, both spectra remain compatible to each other when their (large) experimental uncertainties are taken into account.

Let us now confront our measurements to results obtained numerically. A first global comparison between experimental and theoretical results can be made by determining the zeroth- and second-order moments. With the spectral intensities $I_{\rm iso}(\nu)$ in cm^6 as input we are able to deduce these moments M_0 and M_2 through the following analytical expression:

$$M_{2p} = \left(\frac{\lambda_0}{2\pi}\right)^4 \int_{-\infty}^{+\infty} (2\pi c\nu)^{2p} I_{\rm iso}(\nu)\, d\nu, \tag{6}$$

where λ_0 denotes the laser wavelength and p is a nonnegative integer. In our experiment, only the Stokes spectral side is recorded. The anti-Stokes part of the spectrum is deduced by means of the *detailed balance principle*. It is to be

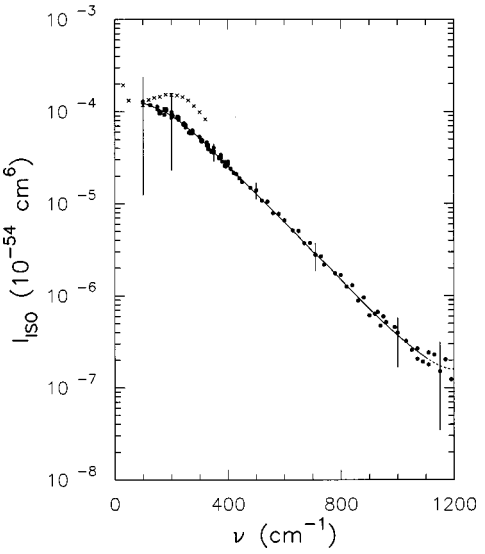

FIG. 3. Isotropic CILS spectrum $I_{\rm iso}(\nu)$ on an absolute scale (cm^6), as a function of frequency ν. The points refer to our experiment. The solid line curve results from the best fit of our measurements as a guide to the eye. The data obtained previously between 20 cm^{-1} and 320 cm^{-1} by Proffitt *et al.* [9] is represented by crosses.

TABLE I. Isotropic experimental intensities expressed on an absolute scale (cm^6), for representative values of ν in the 100–1200 cm^{-1} spectral range, at $T = (294.5 \pm 1)$ K.

ν (cm^{-1})	$I_{\rm iso}(10^{-58}\,cm^6)$	ν (cm^{-1})	$I_{\rm iso}(10^{-58}\,cm^6)$
100	1.24	600	0.630×10^{-1}
120	1.18	650	0.439×10^{-1}
140	1.12	700	0.302×10^{-1}
160	1.05	750	0.217×10^{-1}
180	0.979	800	0.149×10^{-1}
200	0.901	850	0.103×10^{-1}
250	0.697	900	0.720×10^{-2}
300	0.512	950	0.512×10^{-2}
350	0.365	1000	0.371×10^{-2}
400	0.257	1050	0.276×10^{-2}
450	0.181	1100	0.213×10^{-2}
500	0.127	1150	0.174×10^{-2}
550	0.897×10^{-1}	1200	0.159×10^{-2}

TABLE II. Isotropic zeroth-order M_0 and second-order M_2 moments, and second dielectric virial coefficient B_ε. The anti-Stokes spectral intensities were deduced from the measured Stokes intensities via the *detailed balance principle*. To assess the values of M_0 and M_2 from the experiment, extrapolation of our experimental intensities was made by scaling the spectral distribution calculated with the MHWA model in the interval $0 \leqslant \nu \leqslant 100\ \mathrm{cm}^{-1}$. Parentheses denote estimated values.

	$M_0(10^{-4}\ \text{Å}^9)$	$M_2(10^{23}\ \text{Å}^9\ \mathrm{sec}^{-2})$	$B_\varepsilon(10^{-2}\ \mathrm{cm}^6\ \mathrm{mol}^{-2})$
	Experiment[1] (This work) (2.6)	Experiment[1] (This work) 3.2 ± 1.3	Experiment[2] (Previous works) -5.9 ± 0.9[a] -6.0 ± 1.0[b]
Model	Calculations[1]	Calculations[1]	Calculations[2]
MHWA	2.43	3.09	−5.96
BD	2.63	3.13	−6.62
DF	2.56	3.01	−6.29
PKF	3.95	6.32	−7.60
FC	3.60	3.73	−9.13
CF	0.27	0.23	+4.04

[1] $T = 294.5$ K.
[2] $T = 303$ K.
[a] Reference [41].
[b] Reference [42].

noted that the contribution of the high-frequency scattered intensities to the moment M_{2p} increases monotonically with increasing p. In spite of the fact that high-order moments would in principle be more sensitive probes for testing the far spectral wing, the large experimental uncertainties in the high-frequency part of the spectrum reduces the reliability of such a procedure and makes practically useless any moment with $p > 1$. On the other hand, the evaluation procedure of M_0 suffers from the absence of reliable experimental data in the low-frequency domain, as well as from the interpolation error in the vicinity of $\nu = 0$. Table II gives the values of M_0 and M_2 estimated from experimental intensities as well as those calculated from the incremental trace models $\Delta\alpha(r)$ through the expressions [39]:

$$M_0 = 4\pi \int_0^\infty (\Delta\alpha)^2 e^{-V(r)/k_B T} r^2 dr, \tag{7}$$

$$M_2 = 4\pi \frac{k_B T}{\mu} \int_0^\infty \left(\frac{d(\Delta\alpha)}{dr} \right)^2 e^{-V(r)/k_B T} r^2 dr. \tag{8}$$

What is found is that the theoretical values of M_0 and M_2 resulting from the MHWA, BD, and DF incremental trace models are in good agreement with our experimental moments. For the latter calculations the SAPT1 interaction potential is employed. The influence of the potential model is, however, not found to be significant since variations of M_0 and M_2 amount to less than 0.5% for all the *ab initio* models of $V(r)$.

Another way to test the theoretical incremental trace models available in the literature is to confront the resulting spectra to our experimental intensities. For this purpose, Fig. 4 illustrates our experimental isotropic spectrum on an absolute scale, as well as isotropic spectra obtained quantum mechanically by using the aforementioned models. As we can see from this figure, the theoretical spectra computed with the DF, MHWA, and BD incremental trace models are overall compatible with each other. In particular, in the interval 300–1200 cm^{-1}, they are all similar to within less than 5%. It is remarkable that when the uncertainties of the measurements are taken into account these spectra agree well with our experimental intensities throughout the entire spectral domain. Although at low frequencies the agreement with the FC model is less satisfactory, in the interval 300–800 cm^{-1}

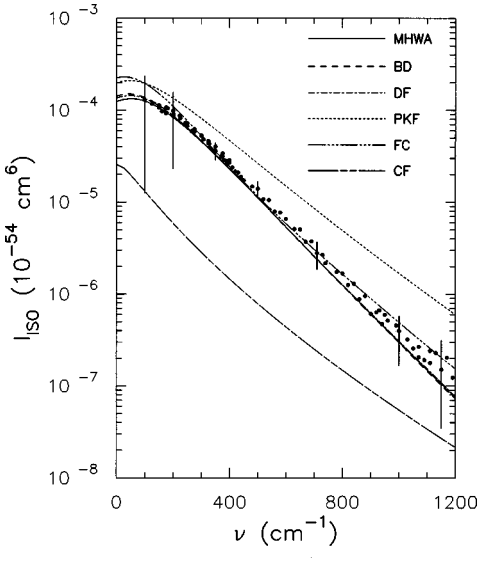

FIG. 4. Comparison between our experimental isotropic spectrum and those obtained quantum mechanically. The points refer to our experiment. Curves refer to spectra computed with the following incremental trace models: CF, FC, PKF, DF, BD, and MHWA.

(where the experimental errors are small) this model well reproduces our measurements, since its deviations from the experiment amount to less than 11%. In the same frequency range, the MHWA, DF, and BD spectra lie systematically below the average experimental intensities by 10–18 %. Besides, it is found that for frequencies above 300 cm^{-1} the PKF model is incompatible with our experiment, while for the CF model the spectrum is incompatible with our experiment at all frequencies.

Although the spectroscopic method used in this work is a quite powerful tool because we compare the shapes of the two spectral distributions on an absolute intensity scale, the straightforward measurement of the second dielectric virial coefficient B_ε is a complementary tool. By simply comparing two numbers, that is the measured and a computed B_ε, this quantity can serve as a sensitive probe for checking the quality of an incremental trace model. This is done by using the following formula [40]:

$$B_\varepsilon = \frac{8\pi^2}{3} N_A^2 \int_0^\infty (\Delta\alpha) e^{-V(r)/k_B T} r^2 dr, \tag{9}$$

where N_A is Avogadro's number. As we can see in Table II, the comparison of experimental values of B_ε available in the literature [41,42] with theoretical ones validates three incremental trace models out of the six checked in this work; these are the ones denoted by MHWA, BD, and DF. This conclusion perfectly meets the one drawn from the comparison between our experimental and theoretical spectra, as we can see in Fig. 4.

Figure 5 displays the contribution to the spectrum of the different partial terms pertaining to the MHWA incremental trace model $\Delta\alpha_{\mathrm{MHWA}}$. The spectrum I_{iso} is built from the sum of all the direct contributions, i.e., those due to the *polarization*, to the *exchange*, to the *induction*, and to the *dispersion*, plus the *cross term* contributions coming from their couplings. While the *direct terms* provide a positive contribution to the spectral intensity, the *cross terms* give a negative contribution. As is shown in Fig. 5, the total MHWA isotropic spectrum scales (over the entire spectral domain) like the dominant partial contributions, that is the contributions due to the *exchange* term and its negative couplings with the rest of the trace components. Again, the frequency dependence of the *polarization* term scales like that of the total intensity; however this term is too weak to play a significant role. The good agreement between experiment and theory is ascertained once again throughout the entire frequency domain.

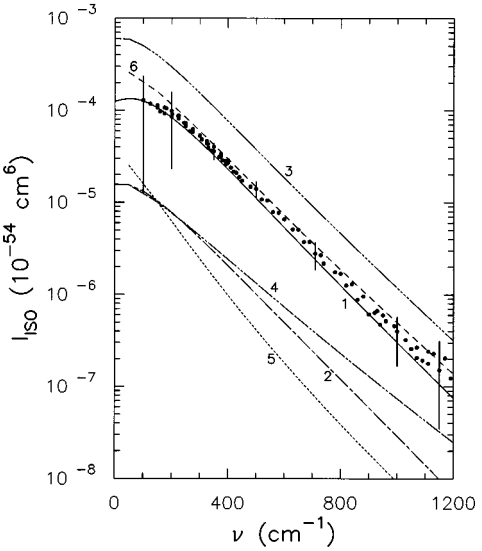

FIG. 5. Partial contributions to the helium isotropic spectrum computed with the MHWA incremental trace model. Curve 1, the total spectrum; curves 2–6, partial contributions to the curve 1 (2, *polarization*; 3, *exchange*; 4, *induction*; 5, *dispersion*; 6, *cross terms* corresponding to ''negative intensities''). The total spectrum (curve 1) is built from the sum of all direct contributions (curves 2–5) minus twice the *cross terms* (curve 6). Our measurements, indicated by points, are also illustrated for comparison.

VI. CONCLUSION

We have measured the He_2 polarized collision-induced light scattering intensities in the spectral range 5–1200 cm^{-1} and then deduced the isotropic CILS spectrum in the interval $\nu = 100-1200\,cm^{-1}$ on an absolute scale. The great extension of the spectral domain, which was probed experimentally, has been accomplished by means of a multichannel CCD camera, able to observe, in the far spectral wing, signals as weak as 1 photoelectron per week and per pixel. A comparison has been made between our experimental intensities and spectra computed quantum mechanically with incremental trace models available in the literature. Analysis of our findings has enabled us to validate certain *ab initio* models, which were found to well reproduce our data. In particular, the conclusion has been drawn that, throughout the entire frequency domain probed, it is the *exchange* component of the incremental trace and its cross term that mainly account for the spectral intensities.

ACKNOWLEDGMENT

We are grateful to Professor R. Moszynski and Professor Ad van der Avoird for providing us with their refined parameters for generating the MHWA incremental trace.

[1] L. Frommhold, Adv. Chem. Phys. **46**, 1 (1981).

[2] *Phenomena Induced by Intermolecular Interactions*, NATO Advanced Study Institute, Series B: Physics, Vol. 127, edited by G. Birnbaum (Plenum, New York, 1985).

[3] *Collision- and Interaction-Induced Spectroscopy*, NATO Advanced Study Institute, Series C: Mathematical and Physical Sciences, Vol. 452, edited by G. C. Tabisz and M. N. Neuman (Kluwer, Dordrecht, 1995).

[4] L. Frommhold and M. H. Proffitt, J. Chem. Phys. **74**, 1512 (1981).
[5] O. Gaye, M. Chrysos, V. Teboul, and Y. Le Duff, Phys. Rev. A **55**, 3484 (1997).
[6] M. H. Proffitt and L. Frommhold, Phys. Rev. Lett. **42**, 1473 (1979).
[7] M. H. Proffitt and L. Frommhold, J. Chem. Phys. **72**, 1377 (1980).
[8] M. H. Proffitt, J. W. Keto, and L. Frommhold, Phys. Rev. Lett. **45**, 1843 (1980).
[9] M. H. Proffitt, J. W. Keto, and L. Frommhold, Can. J. Phys. **59**, 1459 (1981).
[10] R. Wiebe, V. L. Gaddy, and C. Heins, J. Am. Chem. Soc. **53**, 1721 (1931).
[11] R. Wiebe and V. L. Gaddy, J. Am. Chem. Soc. **60**, 2300 (1938).
[12] B. J. Berne and R. Pecora, *Dynamic Light Scattering* (Wiley, New York, 1976).
[13] P. D. Dacre and L. Frommhold, J. Chem. Phys. **76**, 3447 (1982).
[14] P. D. Dacre, Mol. Phys. **45**, 17 (1982).
[15] D. P. Bishop and M. Dupuis, Mol. Phys. **88**, 887 (1996).
[16] R. Moszynski, T. G. A. Heijmen, P. E. S. Wormer, and Ad van der Avoird, J. Chem. Phys. **104**, 6997 (1996).
[17] P. R. Certain and P. J. Fortune, J. Chem. Phys. **55**, 5818 (1971).
[18] P. J. Fortune and P. R. Certain, J. Chem. Phys. **61**, 2620 (1974).
[19] D. W. Norcross and M. J. Seaton, J. Phys. B **6**, 614 (1973).
[20] M. Chrysos and R. Lefebvre, J. Phys. B **26**, 2627 (1993).
[21] M. Chrysos, O. Gaye, and Y. Le Duff, J. Phys. B **29**, 583 (1996).
[22] M. Chrysos, O. Gaye, and Y. Le Duff, J. Chem. Phys. **105**, 1 (1996).
[23] J. O. Hirschfelder, C. F. Curtiss, and R. B. Bird, *Molecular Theory of Gases and Liquids* (Wiley, New York, 1966).
[24] R. A. Aziz, A. R. Janzen, and M. R. Moldover, Phys. Rev. Lett. **74**, 1586 (1995).
[25] R. A. Aziz and M. J. Slaman, J. Chem. Phys. **94**, 8047 (1991).
[26] A. R. Janzen and R. A. Aziz, J. Chem. Phys. **107**, 914 (1997).
[27] T. Korona, H. L. Williams, R. Bukowski, B. Jeziorski, and K. Szalewicz, J. Chem. Phys. **106**, 5109 (1997).
[28] R. J. Gdanitz, Mol. Phys. **96**, 1423 (1999).
[29] The pressure is measured with two sensors. The first is operational in the domain 0–100 bars with a precision that amounts to 0.5%, while the second is within 0–600 bars with a precision amounting to 1%.
[30] During the registration a statistical test is made, handling five (or more) signal measurements.
[31] P. M. Lallemand, Phys. Rev. Lett. **25**, 1079 (1970).
[32] B. P. Stoicheff, Can. J. Phys. **35**, 730 (1957).
[33] J. Rychlewski, J. Chem. Phys. **78**, 7252 (1983); C. Schwarz and R. J. Le Roy, J. Mol. Spectrosc. **121**, 420 (1987).
[34] C. Adjouri, A. Elliasmine, and Y. Le Duff, Spectroscopy **11**, 45 (1996).
[35] B. Yang, M. D. Morris, and H. Owen, Appl. Spectrosc. **45**, 1533 (1991).
[36] M. J. Pelletier and R. C. Reeder, Appl. Spectrosc. **45**, 765 (1991).
[37] C. Guillot-Noël, M. Chrysos, Y. Le Duff, and F. Rachet, J. Phys. B **33**, 569 (2000).
[38] F. Rachet, M. Chrysos, C. Guillot-Noël, and Y. Le Duff, Phys. Rev. Lett. **84**, 2120 (2000).
[39] H. B. Levine and G. Birnbaum, J. Chem. Phys. **55**, 2914 (1971).
[40] A. D. Buckingham and J. A. Pople, Trans. Faraday Soc. **51**, 1029 (1955).
[41] S. Kirouac and T. K. Bose, J. Chem. Phys. **64**, 1580 (1976).
[42] H. J. Achtermann, J. G. Hong, G. Magnus, R. A. Aziz, and M. J. Slaman, J. Chem. Phys. **98**, 2308 (1993).